INTL JOURNAL OF ELECTRONICS AND TELECOMMUNICATIONS, 2026, VOL. 72, NO. 2, PP. 1-7
Manuscript received November 14, 2025; revised April 2026. doi: 10.24425/ijet.2026.157914

Small-signal model of RF InAlGaN/GaN HEMT and on-chip calibration structures

Martin Florovič, Michal Dzuriš, Jakub Krchnák, Aleš Chvála, Jaroslav Kováč, jr., Soňa Kováčová, Jaroslav Kováč, René Harťanský, Ľubica Stuchlíková, and Matej Matuš

***Abstract*—The advanced GaN-based devices utilized for high-performance radio frequency (RF) applications are intensively studied to be used as RF sensors or amplifiers. The paper is focused on microwave characterization of two port passive devices, especially on-chip calibration structures and InAlGaN/GaN electron mobility transistor (HEMT) operating in the cold bias region (zero applied voltage). The acquired S-parameters are inputs to build a passive device small-signal model consisting of three star-connected impedances. The calculated Z-parameters are possible to be utilized for on-chip signal paths design. The parameters to be calculated are assumed frequency independent, however, more proper HEMT modelling requires non-zero voltage application, therefore, the model possibilities are depicted and discussed.**

***Keywords*—GaN; HEMT; RF on-chip calibration; S-parameters; Z-parameters; small-signal model**

I. Introduction

GaN-based devices offer superior performance in high-power, high-frequency and high-temperature applications due to wide-bandgap, high current density and electron mobility caused by the generation of its unique 2-D electron gas [1,2]. High electron mobility transistors (HEMTs) have been widely studied and utilized in high-frequency power amplifiers [3,4]. Recently, with the commercialization of 5G communication and signal detection research on millimeter-wave power gigahertz (GHz) electronics is being actively developed. The device large-signal modeling reflects non-linear effects up to the millimeter-wave band, self-heating, device trapping and degradation effects are considered as well [5,6]. Although device large-signal modeling reflects self-heating effects up to the millimeter-wave band, to explain radio frequency (RF) phenomena, a small-signal model is prioritized as the frequency increases reflecting frequency dependent device S-parameters and Z-parameters [7-9]. However, temperature dependent DC and AC electric parameters acquisition allows to build up the large-signal model possible to be employed in the device transient analysis [10,11].

The vector network analyzer (VNA) as a precision measuring tool requires RF calibration using a vector error correction to remove systematic errors' contribution coming out from absorption, delay or phase shift of the signal path from the VNA generator/detector to the device under test (DUT) as depicted in Fig. 1.

The electrical standards used during the RF calibration process can be the well-known SHORT, OPEN, LOAD and THRU (SOLT) utilizing the calibration substrate to correct VNA to probe tips signal paths which may differ in general due to various coaxial cable lengths, bending, connectors, etc. Those signal paths are high-distance in comparison to the RF signal wavelength, therefore the small-signal model of distributed parameters is required to be utilized for the coaxial cable, connectors and probes. The small-signal model of lumped parameters can be employed for a large wavelength signal [12].

Whereas standard materials and metallization used for fabrication of conventional test semiconductor structures suffer from imperfections in their electrical and spatial parameters, various signal paths are utilized for on-chip calibration. OPEN, SHORT and THRU test structures of the vertical and horizontal dimensions similar to the DUT dimensions offer acceptable compromise between broadband and low-space on-chip calibration to correct signal paths from probe tips to DUT [13]. The pad paths are usually considered as similar, the test structures are symmetrical and low-distance in comparison to the RF signal wavelength and hence the small-signal model of lumped parameters can be utilized.

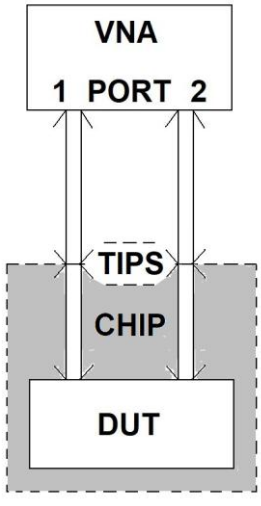

Fig. 1. Block diagram of RF measurement.

This work was supported from the projects 1/0480/24 of VEGA grant agency and APVV-21-0365 from Slovak Research and Development Agency, all of Ministry of Education, Science, Research and Sport of the Slovak Republic.).

Martin Florovič, Aleš Chvála, Jaroslav Kováč, jr., Soňa Kováčová, , Jaroslav Kováč, Ľubica Stuchlíková and Matej Matuš are with Institute of Electronics and Photonics, Faculty of Electrical Engineering and Information Technology, Slovak University of Technology (e-mail: martin.florovic@stuba.sk).

Michal Dzuriš, Jakub Krchnák and René Harťanský are with Institute of Electrical Engineering, Faculty of Electrical Engineering and Information Technology, Slovak University of Technology.

The paper deals with the microwave characterization of InAlGaN/GaN (HEMT) and on-chip two port calibration structures in the operation frequency range 10 MHz to 40 GHz. The obtained S-parameters were utilized as input parameters to create simplified small signal model of the investigated HEMT at zero applied DC voltage [14]. The measured S-parameters [15] are employed to create the small-signal model of on-chip calibration structures as the cascade connection of pad path and short/open/line path.

In this case, HEMT and calibration structure act as a passive two port device, therefore three star-connected impedances can be employed to form the small-signal model. S-parameters to Z-parameters conversion in the forward and reverse way is used to calculate and verify small-signal model parameters. The model properties and on-chip calibration planes are discussed and compared to the advanced HEMT small-signal equivalent circuit in the cold bias region [9] useful for establishing initial values for voltage-dependent models.

II. Theory

In Fig. 1 all blocks/paths are characterized by S-parameter matrixes utilizing signal power – input a_1, a_2 and output b_1, b_2 as shown in Fig. 2. In the block diagram, VNA S-parameter matrix is supposed zero and the VNA port reflection and crosstalk are included in the VNA to tips path, which act as active devices, in general non-symmetrical and non-reciprocal.

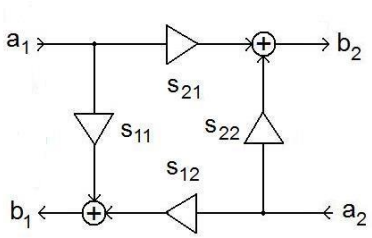

Fig. 2. Block diagram of two-port blocks/paths in Fig. 1.

Tips to DUT paths and DUT are characterized by the electric model of lumped parameters. Thus, in this case two-port S-parameters (s_{11}, s_{21}, s_{12}, s_{22}) conversion to Z-parameters (z_{11}, z_{21}, z_{12}, z_{22}) utilizing characteristic impedance Z_0 [8] gives possibility to find a small-signal model shown in Fig. 3 utilizing incident port currents I_1, I_2 and voltages V_1, V_2.

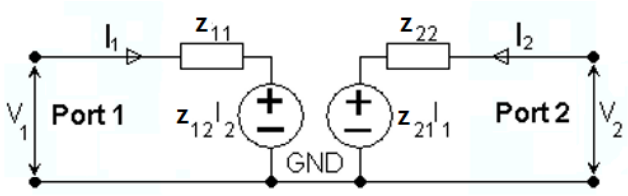

Fig. 3. Generalized small-signal model.

In Fig. 3 the parameters z_{11}, z_{22} are modelled by impedances of voltage drop $z_{11}I_1$, $z_{22}I_2$ caused by currents I_1, I_2 flowing directly through the impedance. However, parameters z_{12}, z_{21} are modelled by voltage sources of drop $z_{12}I_2$, $z_{21}I_1$ driven by currents I_1, I_2 not flowing through them, therefore the incident signal can be gained due to external power application not depicted in the small-signal model.

Most passive components like resistors, capacitors, inductors are reciprocal resulting in $s_{12} = s_{21}$, except for structures involving magnetized ferrites, plasmas, etc. This is also valid for passive devices consisting of frequency dependent passive components, e.g. HEMT gate capacitance. Coming out from the definition, a two-port passive circuit exhibits the sum of the reflected and transmitted wave power equal to or less than the incident wave power. The two-port passive device model of lumped electric parameters consists of the parallel and serial combination of resistors, capacitors, and inductors only. However, the sources of voltage $z_{12}I_2$, $z_{21}I_1$ driven by external currents I_2, I_1, respectively, are present in the small-signal model in Fig. 3. To solve this, a small-signal model consisting of three star-connected impedances was utilized as depicted in Fig. 4 with the following parameters:

$$Z_{GND} = z_{12} = z_{21} \quad (1)$$

$$Z_1 = z_{11} - z_{12} \quad (2)$$

$$Z_2 = z_{22} - z_{12} \quad (3)$$

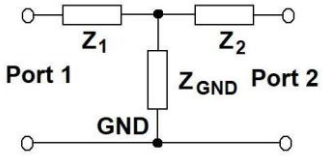

Fig. 4. Small-signal model of three star-connected impedances.

Coming out from the S-parameter matrix conversion to Z-parameter matrix, reciprocal components exhibit $s_{12} = s_{21}$ and $z_{12} = z_{21}$. Hence, if experimentally acquired s_{12}, s_{21} exhibit a similar frequency dependence, the small-signal model of three star-connected impedances can be utilized, no additional assumptions are required.

III. Experimental

The VNA Agilent Technologies E8363B was utilized to acquire S-parameters in the frequency range 10 MHz to 40 GHz. The VNA DC input of the built-in mixer was grounded during the measurements to ensure zero DC voltage connected. The block diagram of RF measurement setup is shown in Fig. 1 taking signal paths into account.

The error correction of the VNA to probe tips signal paths was realized by SOLT calibration utilizing built-in software and algorithms. Pico-probes and calibration substrate with the calibration protocol were obtained from GGB Industries.

The InAlGaN/GaN HEMT structure consists of ~ 800 nm thick GaN buffer layer grown on a SiC substrate followed by a patented ~ 800 nm thick AlGaN back barrier, ~ 150 nm thick GaN layer, AlN interlayer and top InAlGaN barrier of thickness ~ 6 nm.

The structure was processed by standard Au metallization to form OPEN, SHORT, THRU calibration structures of the horizontal dimensions similar to the investigated HEMT dimensions as shown in Fig. 5. Double gated HEMT of device width ~ 50 μm, gate length ~ 1.5 μm and optimized gate to source and gate to drain gap length in the range 1 μm to 2 μm was investigated. The chip was placed on the Al chuck during RF measurements.

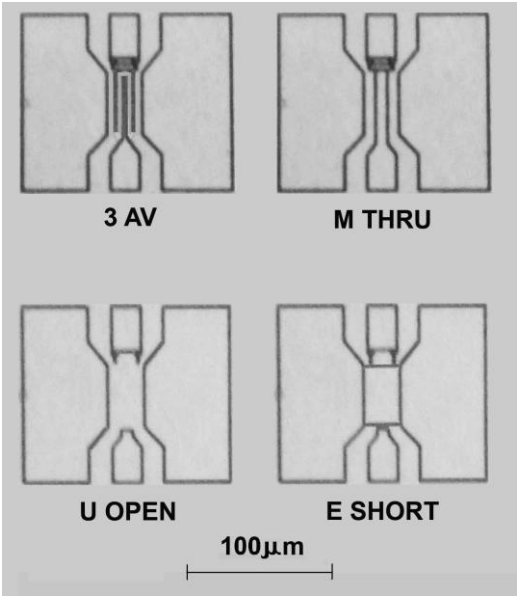

Fig. 5. Horizontal view on double gated InAlGaN/GaN HEMT and calibration structures.

IV. Results and Discussion

1) InAlGaN/GaN HEMT

The widely utilized small-signal equivalent circuit of GaN-based HEMTs is shown in Fig. 6 indicating the port numbers, the source is connected to the ground [9]. The model consists of pad parasitic capacitances (C_{pg}, C_{pd}) and pad parasitic inductances (L_{pg}, L_{pd}), an extrinsic part depending on the layout structure and independent of applied voltage and an intrinsic part of parameters changing by applied biases [16,17]. The extrinsic part consists of the source, drain and gate series resistances R_s, R_d, R_g, the source, drain and gate series inductances L_s, L_d, L_g. The R_{ds} and C_{ds} are usually classified as intrinsic model parameters, but empirically, the difference in values extracted according to biases is not large [16,17]. The intrinsic part contains the gate to drain impedance source consisting of R_{gd}, C_{gd}, and the gate to source impedance consisting of R_i and C_{gs}, those parameters are voltage dependent. The active part of the circuit in Fig. 6. is the current source of complex transconductance G_m driven by the intrinsic gate to source voltage V_{igs}. Despite the zero DC voltage was connected to the investigated HEMT during RF measurements, the circuit and parameters mentioned above are crucial to utilize small-signal models of RF signal paths on chip.

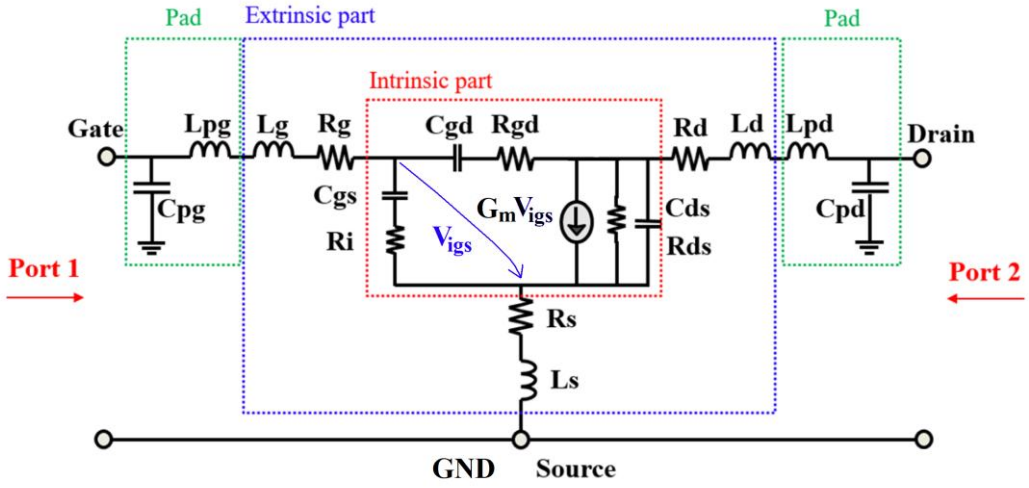

Fig. 6. Conventional small-signal equivalent circuit of a GaN-based HEMT [9].

2) On-chip Calibration Structures

The small-signal model is utilized to find impedances Z_1, Z_2 and Z_{GND} of pad path and particular path connected in the cascade resulting in RF on-chip test structure. Both pad paths (P) are supposed to be the same characterized by S-parameters $s_{11}{}^P$, $s_{22}{}^P$, $s_{21}{}^P$, $s_{12}{}^P$. Therefore, on-chip calibration is based on simplified SOLT calibration, utilizing OPEN, SHORT, THRU structures, and LOAD structure is not required.

To avoid robust calculations and numerous calibration structures, DUT in Fig. 1 is set as ideal open, short and line structure. Two-port open path of the test structure OPEN is characterized by:

$$s_{11}^O = s_{22}^O = 1 \quad s_{12}^O = s_{21}^O = 0 \tag{4}$$

$$Z_1^O = Z_2^O = \infty \quad Z_{GND}^O = 0 \tag{5}$$

The two-port open path of the test structure SHORT is characterized by:

$$s_{11}^S = s_{22}^S = -1 \quad s_{12}^S = s_{21}^S = 0 \tag{6}$$

$$Z_1^S = Z_2^S = 0 \quad Z_{GND}^S = 0 \tag{7}$$

The two port line path (L) of the test structure THRU is supposed as coplanar line characterized by:

$$s_{11}^L = s_{22}^L = 0 \quad s_{12}^L = s_{21}^L \tag{8}$$

The S-parameters of on-chip calibration structures shown in Fig. 7 are utilized to build a small-signal model of RF paths [15].

The impedance/admittance pad path parameters $Z_1{}^P$, $Z_2{}^P$, and $Y_{GND}{}^P = (Z_{GND}{}^P)^{-1}$ were calculated by S-parameters to Z-parameters conversion and utilizing (1), (2), and (3). The constant real part and imaginary part linearly dependent on frequency f of the impedances Z_1, Z_2 and admittance $Y_{GND} = Z_{GND}{}^{-1}$, respectively, were supposed to find the corresponding resistances R, conductivities G and inductances $L = Im\{Z\}/2\pi f$, $L = Im\{Y\}/2\pi f$, respectively, utilizing operating frequency f.

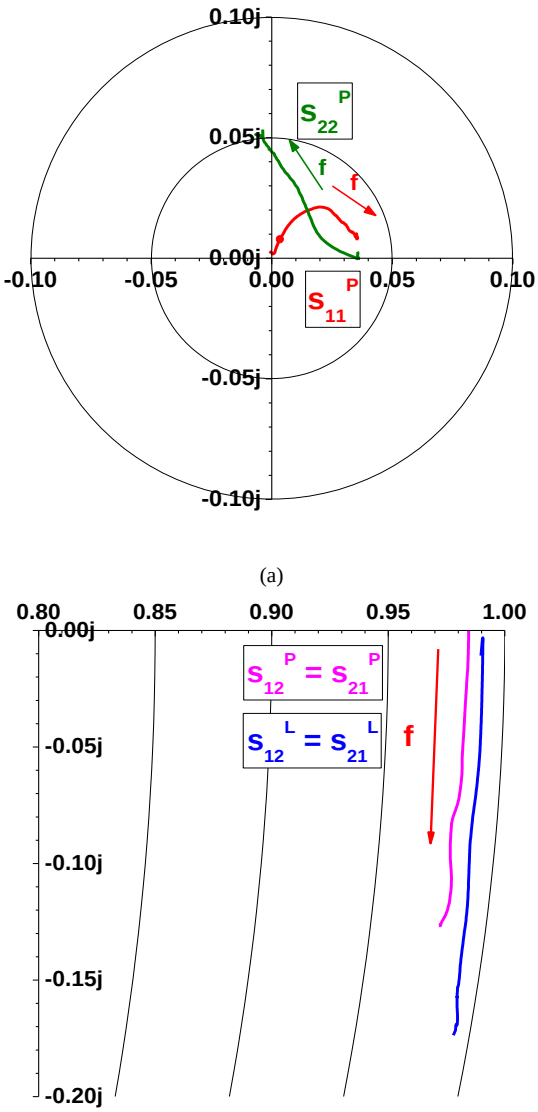

Fig. 7. S-parameters of pad path and line path of on-chip test structure
a) $s_{11}{}^{P}$ and $s_{22}{}^{P}$ of pad part
b) $s_{21}{}^{P} = s_{12}{}^{P}$ of pad path and $s_{21}{}^{L} = s_{12}{}^{L}$ of line path.

The pad path impedances and admittance are shown in Fig. 8 divided into real and imaginary parts. Due to a small difference of $s_{11}{}^{P}$ and $s_{22}{}^{P}$, $Z_1{}^{P}$ is close to $Z_2{}^{P}$, therefore, the pad path exhibits symmetrical passive device properties.

The parameters of the gate pad and the drain pad in Fig. 6 are defined as follows:

$$z_{11} = z_{12} = z_{21} = \left(j\omega C_{pg}\right)^{-1} \quad (9)$$

$$z_{22} = j\omega L_{pg} + \left(j\omega C_{pg}\right)^{-1} \quad (10)$$

However, the model in Fig. 6 does not cover the pad path resistance and conductance, moreover, the contact tips resistance difference between investigated and calibration substrate is not included. Therefore, RF pad path parameters are better fulfilled utilizing model of three-star-connected impedances in Fig. 4.

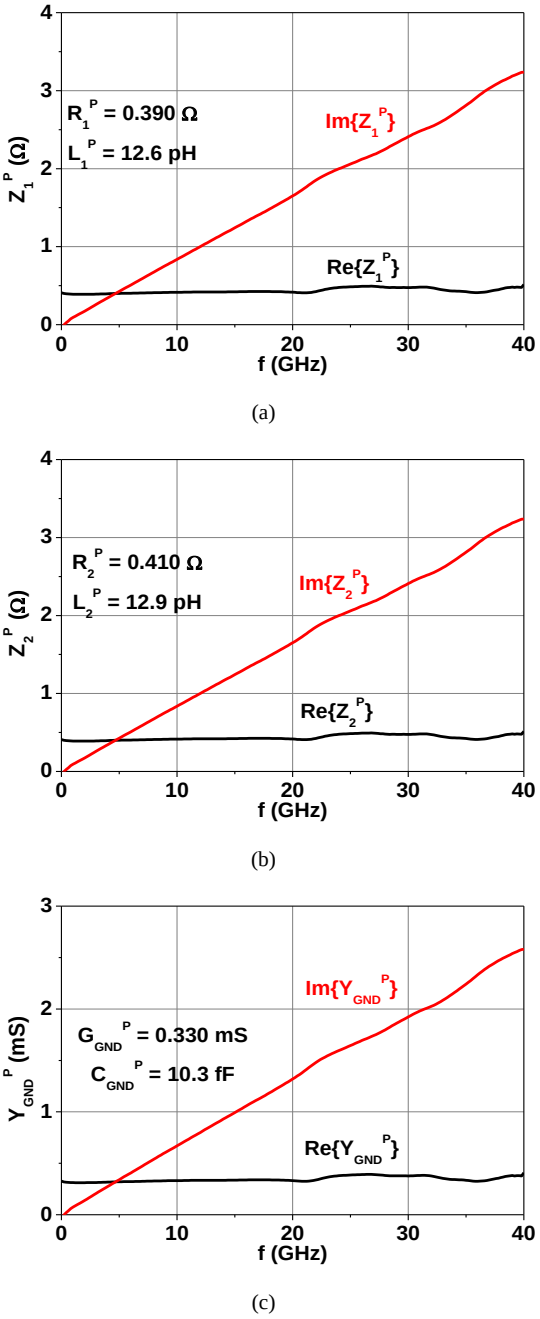

Fig. 8. Pad path of RF on-chip test structure – real and imaginary part frequency dependence of
a) impedance $Z_1{}^{P}$ and corresponding resistance $R_1{}^{P}$ and inductance $L_1{}^{P}$
b) impedance $Z_2{}^{P}$ and corresponding resistance $R_2{}^{P}$ and inductance $L_2{}^{P}$
c) admittance $Y_{GND}{}^{P}$ and corresponding conductance $G_{GND}{}^{P}$ and capacitance $C_{GND}{}^{P}$.

For the line path $Z_1{}^{L}$, $Z_2{}^{L}$, and $Y_{GND}{}^{L} = (Z_{GND}{}^{L})^{-1}$ were calculated by S-parameters to Z-parameters conversion and utilizing (1), (2) and (3). The acquired S-parameters result in the same $Z_1{}^{L}$ and $Z_2{}^{L}$. The real and imaginary parts of $Z_1{}^{L} = Z_2{}^{L}$ and $Y_{GND}{}^{L} = (Z_{GND}{}^{L})^{-1}$ shown in Fig. 9 indicate coplanar line segment properties.

The calculations validate the assumption of negligible effective structure permittivity and permeability variation nearby RF on-chip RF paths in the operation frequency range.

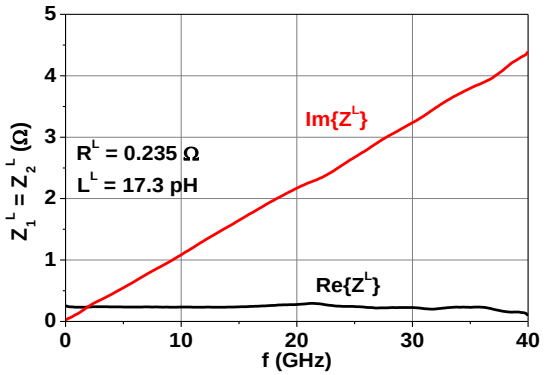

(a)

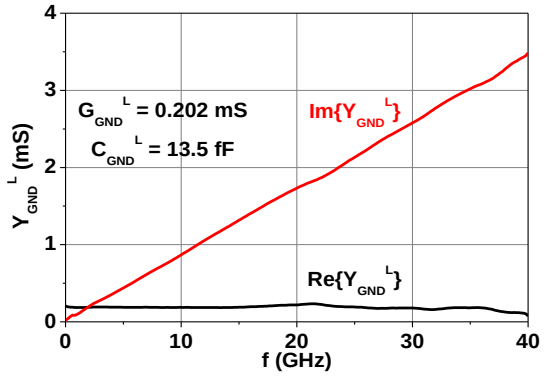

(b)

Fig. 9. Line path of RF on-chip test structure – real and imaginary part frequency dependence of a) impedance $Z_1^L = Z_2^L$ and corresponding resistance R^L and inductance L^L b) admittance Y_{GND}^L and corresponding conductance G^L and capacitance C^L.

3) InAlGaN/GaN HEMT

After de-embedding the pad path model, extrinsic model parameters are possible to be extracted through S-parameters measured in the cold bias region where the drain-source voltage is zero. Based on the conventional small-signal equivalent circuit of a GaN-based HEMT [9] the small-signal equivalent circuit in the cold bias region in Fig. 10 consists of source, drain and gate series resistances R_s, R_d, R_g, source, drain and gate series inductances L_s, L_d, L_g, distributed channel resistance under the gate R_{ch} and distributed gate resistance R_{sdj} and capacitance C_{sdj}. Z-parameters are yielded as the sum of extrinsic model resistances, inductances and intrinsic model resistances, capacitances taking distributed channel parameters into account:

$$z_{11} = R_s + R_g + \left(\frac{R_{ch}}{3}\right) + \left[R_{sdj} \parallel \left(C_{sdj}\right)^{-1}\right] + j\omega\left(L_s + L_g\right) \quad (11)$$

$$z_{12} = z_{21} = R_s + (R_{ch}/2) + j\omega L_s \quad (12)$$

$$z_{22} = R_s + R_d + R_{ch} + j\omega(L_s + L_d) \quad (13)$$

With respect to the small-signal equivalent circuit in Fig. 10 Z-parameters in Fig. 4 are defined as the sum of the following real and imaginary parts:

$$Z_{GND} = R_S + j\omega L_S \quad (14)$$

$$Z_1 = R_G + j\omega L_G + (G_G + j\omega C_G)^{-1} \quad (15)$$

$$Z_2 = R_D + j\omega L_D \quad (16)$$

The relation between parameters in (11), (12), (13) and parameters utilized in (14), (15), (16) are as follows:

$$R_S = R_s + (R_{ch}/2) \quad (17)$$

$$R_D = R_d + (R_{ch}/2) \quad (18)$$

$$R_G = R_g \quad (19)$$

$$G_G + j\omega C_G = \left[R_{sdj} \parallel \left(C_{sdj}\right)^{-1}\right]^{-1} \quad (20)$$

$$L_G = L_g \quad (21)$$

$$L_D = L_d \quad (22)$$

$$L_S = L_s \quad (23)$$

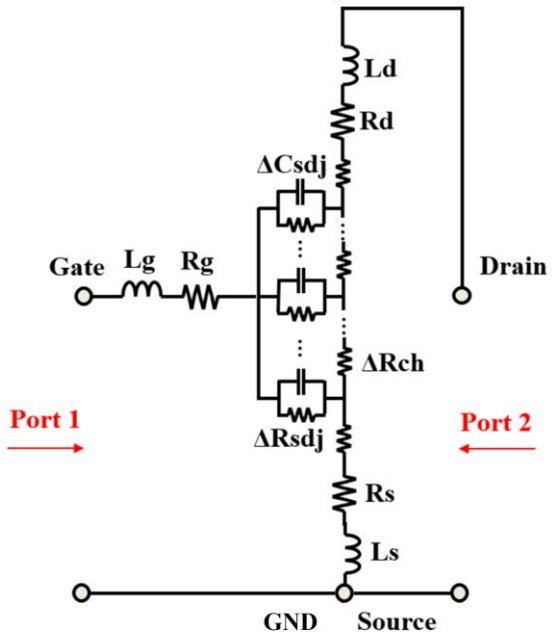

Fig. 10. GaN-based HEMT small-signal equivalent circuit in the cold bias region [9].

The measured S-parameters of investigated HEMT are depicted in Fig. 11 [14]. The condition $s_{21} = s_{12}$ is met and a small-signal model of three star-connected impedances at zero applied voltage in Fig. 4 can be utilized, whereas no voltage sources depicted in Fig. 3. are required. The Z_1, Z_2 and Y_{GND} sub-circuits including approximated resistances, inductances, admittances and capacitances are shown in Fig. 12.

The frequency dependence of the real and imaginary parts of the calculated impedance Z_2, obtained using S-parameters to Z-parameters conversion and (3), shown in Fig. 12 (b), gives the opportunity to determine constant R_D and L_D values along the investigated RF range, since the thin drain contact acts as an inductance. The distributed inductance and resistance along the drain electrode causes the deviation in the Z_2 real part constancy and the Z_2 imaginary part linearity.

Whereas HEMT and on-chip calibration structures are surrounded by GND metallization connected to the source, a notable parallel capacitance C_S coming out of admittance $Y_{GND} = (Z_{GND})^{-1} = (R_S)^{-1} + j\omega C_S$ is depicted in Fig. 12 (c). The additional distributed series impedance causes the notable Y_{GND} real part increase.

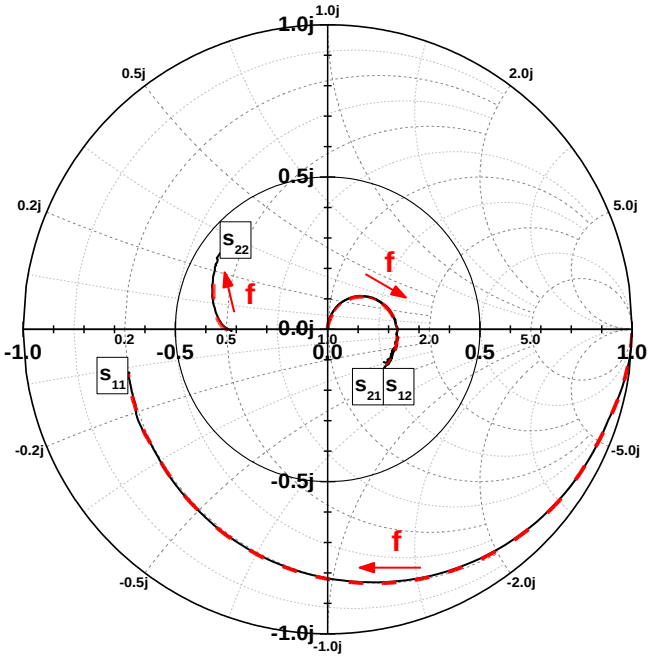

Fig. 11. Measured (black solid curves) and modelled (red dashed curves) S-parameters of investigated InAlGaN/GaN HEMT.

The gate series resistance R_G and inductance L_G cannot be extracted in a simple way as indicated above from Fig. 12 (a) due to the intrinsic gate conductance G_G and capacitance C_G. Due to the symmetrical HEMT design, L_G is supposed to be like L_D and R_G is extracted from the constant real part of Z_1 at high frequencies [7]. The subsequently calculated $G_G \| C_G$ admittance allows to approximate its real and imaginary parts along the investigated RF range and verify whether they are constant and linearly dependent, respectively.

To separate R_s, R_d, and R_{ch} from R_S and R_D, respectively, and to determine G_G and C_G dependent on vertical electric field, non-zero voltage is required to be applied [7,8] and additionally, R_g and L_g can be determined more accurately.

Constant values of resistors, inductors, and capacitors in Fig. 12 underline the negligible effective structure permittivity and permeability variation along the operation frequency range.

The measured and modelled S-parameters depicted in Fig. 4 are in good correspondence. The proposed method is useful to determine initial values for the proper HEMT RF modelling along the operation voltage range.

CONCLUSION

The small-signal model of three star-connected impedances utilized for passive devices was employed to characterize InAlGaN/GaN HEMT and on-chip calibration structures in the frequency range of 10 MHz to 40 GHz. The proposed model was compared to GaN-based HEMT small-signal equivalent circuit parameters in the cold bias region. The frequency dependence of calculated impedances and admittances indicate the real part and the imaginary part close to constant and linearly dependent, respectively, giving an opportunity to employ simple resistors, inductors and capacitors in the device small-signal equivalent circuit.

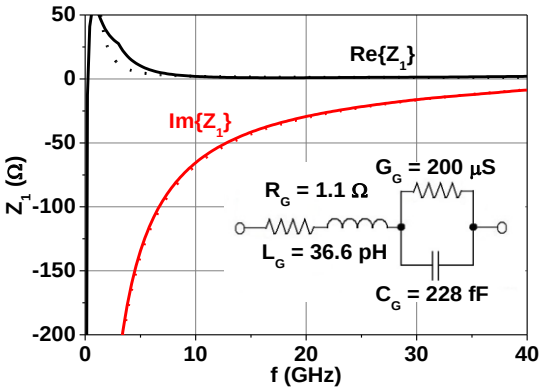

(a)

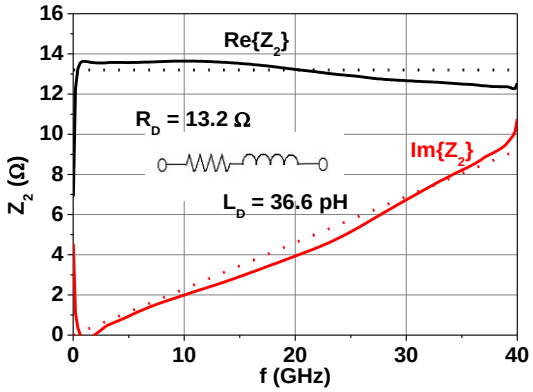

(b)

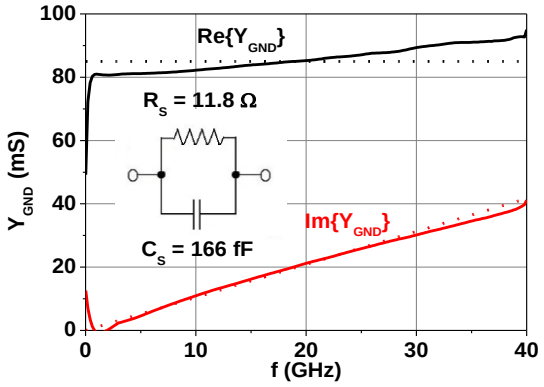

(c)

Fig. 12 Calculated (solid curves) and modelled (dashed curves) impedances: (a) Z_1, (b) Z_2 and (c) admittance Y_{GND} of investigated InAlGaN/GaN HEMT including determined parameters corresponding to the small-signal model sub-circuits.

The model validation exhibits good correspondence between measured and modelled S-parameters, the deviation is caused by additional distributed parameters not involved in the model. The method utilized in the paper is useful to determine initial values for the GaN-based HEMT RF modelling along the operation voltage range. The three star-connected impedances calculation is possible to be employed in the automated measuring system.

ACKNOWLEDGEMENTS

The research leading to these results has received funding from the projects 1/0480/24 of VEGA grant agency and APVV-21-0365 from Slovak Research and Development Agency, all of Ministry of Education, Science, Research and Sport of the Slovak Republic.

REFERENCES

[1] R. S. Pengelly, S. M. Wood, J. W. Milligan, S. T. Sheppard, and W. L. Pribble, "A Review of GaN on SiC High Electron-Mobility Power Transistors and MMICs", IEEE Trans. on Microwave Theory and Techniques, Vol. 60, No. 6, pp. 1764-1783, 2012. https://doi.org/10.1109/TMTT.2012.2187535

[2] Ch.-W. Su, T.-W. Wang, M.-Ch. Wu, Ch.-J. Ko, and J.-B. Huang, "Fabrication and characterization of GaN HEMTs grown on SiC substrates with different orientations", Solid-State Electronics, Vol. 179, 107980, 2021. https://doi.org/10.1016/j.sse.2021.107980

[3] J. Ajayan, and S. Sreejith, "AlGaN/GaN High electron Mobility Transistor (HEMT) based radio frequency power amplifiers for future wireless communication transmitters: Exciting prospects and challenges", Solid-State Electronics, Vol. 179, 107980, 2021.
https://doi.org/10.1016/j.mee.2025.112342

[4] H. Lu, M. Zhang, L. Yang, B. Hou, R. P. Martinez, M. Mi, J. Du, L. Deng, M. Wu, S. Chowdhury, X. Ma, and Y. Hao, "A review of GaN RF devices and power amplifiers for 5G communication applications", Fundamental Research, Vol. 5, Iss. 1, p. 315-331, 2025. https://doi.org/10.1016/j.fmre.2023.11.005

[5] Sh. Awasthi, H.-T. Hsu, Y.-F. Tsao,P.-H. Chiu, and A. Gupta, "A computational approach to optimize the linearity in dual-gate InAlGaN/AlN/GaN HEMTs", Semiconducor Science and Technology, Vol. 39, 125009, 2024. https://doi.org/10.1088/1361-6641/ad8eed

[6] R. P. Martinez, M. Iwamoto, J. Xu, Ch. Gillease, S, Cochran, and M. Culver, "Assessment and Comparison of Measurement-Based Large-Signal FET Models for GaN HEMTs", IEEE Transactions on Microwave Theory and Techniques, Vol. 72, Iss. 5, p. 2692 – 2703, 2024. https://doi.org/10.1109/TMTT.2023.3349172

[7] Z. Zhao, Y. Lu, Ch. Yi, Y. Chen, X. Cai, Y. Zhang, X. Duan, X. Ma, Y. Hao, "A fast small-signal modeling method for GaN HEMTs, Solid-State Electron", Vol. 175, 107946, 2020.
https://doi.org/10.1016/j.sse.2020.107946

[8] Y. Chen, Y. Xu, F. Wang, Ch. Wang, Q. Wu, S. Qiao, B. Yan, and R. Xu, "A scalable and multi-bias parameter extraction method for a small-signal GaN HEMT model", Int. J. Numer. Model, Vol. 31, 2347, 2018. https://doi.org/10.1002/jnm.2347

[9] J. Kim, "New GaN HEMT Small-Signal Model Considering Source via Effects for 5G Millimeter-Wave Power Amplifier", Design. Appl. Sci., Vol. 11, pp. 9120, 2021. https://doi.org/10.3390/app11199120

[10] S.A.Ahsan, S. Ghosh, S. Khandelwal, and Y.S. Chauhan, "Physics-Based Multi-Bias RF Large-Signal GaN HEMT Modeling and Parameter Extraction Flow", IEEE J. Electron Devices Soc., Vol. 5, pp. 310–319, 2017. https://doi.org/10.1109/JEDS.2017.2724839

[11] J. Kim, K. Choi, S. Lee, H. Park, and Y. Kwon, "6–18 GHz Reactive Matched GaN MMIC Power Amplifiers with Distributed L-C Load Matching", J. Electromagn. Eng. Sci., Vol. 16, 16, pp. 44–51, 2016. https://doi.org/10.5515/JKIEES.2016.16.1.44

[12] E. Lourandakis, "Network Analyzer Basics and Calibration", in On-Wafer Microwave Measurements and De-embedding, pp. 33-62. 2016. ISBN: 9781630810566

[13] E. Lourandakis, "On-Wafer De-Embeding Methods", in On-Wafer Microwave Measurements and De-embedding, 2016, pp. 93-118. ISBN: 9781630810566

[14] M. Florovič, M. Dzuriš, J. Kováč, jr. R. Harťanský, A. Chvála, S. Kováčová, and J. Kováč, "The High-Frequency Characterization of InAlGaN/GaN HEMT Utilizing RF Measurements", in 12th International Conference on Advances in Electronic and Photonic Technologies (ADEPT 2024), Podbanské, Slovakia, pp. 49-52, 24-27 June, 2024. ISBN: 9788055419770

[15] M. Florovič, M. Dzuriš, R. Harťanský, J. Kováč, A. Chvála, and D. Gregušová, "Simple RF on-chip calibration for high-frequency transistor measurements", in Proceedings of the 15th International Conference on Advanced Semiconductor Devices and Microsystems (ASDAM '2024), Smolenice, Slovakia, pp. 46-49, 20-23 October, 2024. https://doi.org/10.1109/ASDAM63148.2024.10844608

[16] M. Mußer, F. Raay, P. Brückner, W. Bronner, R. Quay, and M. Mikulla, "Individual source vias for GaN HEMT power bars", in Proceedings of the 2013 European Microwave Integrated Circuit Conference, Nuremberg, Germany, pp. 184–187, 6–8 October 2013. ISBN:978-2-87487-032-3

[17] G. Dambrine, A. Cappy, F. Heliodore, and E. Playez, "A new method for determining the FET small-signal equivalent circuit", IEEE Trans. Microw. Theory Tech., Vol. 36, pp. 1151–1159, 1988. https://doi.org/10.1109/22.3650